analytical chemistry

pubs.acs.org/ac

Article

Multiplexed and High-Throughput Label-Free Detection of RNA/Spike Protein/IgG/IgM Biomarkers of SARS-CoV-2 Infection Utilizing Nanoplasmonic Biosensors

Adrianna N. Masterson, Barry B. Muhoberac, Adnan Gopinadhan, David J. Wilde, Frédérique T. Deiss, Chandy C. John, and Rajesh Sardar*

Cite This: *Anal. Chem.* 2021, 93, 8754−8763

Read Online

ACCESS | Metrics & More | Article Recommendations | Supporting Information

ABSTRACT: To tackle the COVID-19 outbreak, which is caused by severe acute respiratory syndrome coronavirus 2 (SARS-CoV-2), there is an unmet need for highly accurate diagnostic tests at all stages of infection with rapid results and high specificity. Here, we present a label-free nanoplasmonic biosensor-based, multiplex screening test for COVID-19 that can quantitatively detect 10 different biomarkers (6 viral nucleic acid genes, 2 spike protein subunits, and 2 antibodies) with a limit of detection in the aM range, all within one biosensor platform. Our newly developed nanoplasmonic biosensors demonstrate high specificity, which is of the upmost importance to avoid false responses. As a proof of concept, we show that our detection approach has the potential to quantify both IgG and IgM antibodies directly from COVID-19-positive patient plasma samples in a single instrument run, demonstrating the high-throughput capability of our detection approach. Most importantly, our assay provides receiving operating characteristics, areas under the curve of 0.997 and 0.999 for IgG and IgM, respectively. The calculated *p*-value determined through the Mann−Whitney nonparametric test is <0.0001 for both antibodies when the test of COVID-19-positive patients (n = 80) is compared with that of healthy individuals (n = 72). Additionally, the screening test provides a calculated sensitivity (true positive rate) of 100% (80/80), a specificity (true negative rate) >96% (77/80), a positive predictive value of 98% at 5% prevalence, and a negative predictive value of 100% at 5% prevalence. We believe that our very sensitive, multiplex, high-throughput testing approach has potential applications in COVID-19 diagnostics, particularly in determining virus progression and infection severity for clinicians for an appropriate treatment, and will also prove to be a very effective diagnostic test when applied to diseases beyond the COVID-19 pandemic.

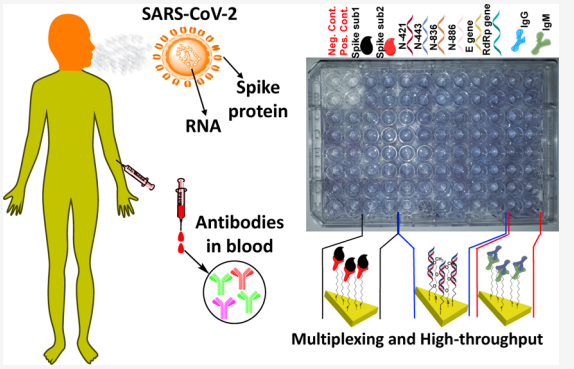

INTRODUCTION

Both human lives and the global economy have been severally damaged from the ravages of the 2019 Coronavirus (COVID-19) pandemic. Global activity is disrupted or paused, and severe acute respiratory syndrome coronavirus 2 (SARS-CoV-2) has caused more than 70 million infections and >1.6 million deaths worldwide.[1] Since this pandemic has started, the scientific community has come together to provide ways to stop the spread of this highly contagious virus through prevention (i.e., developing a vaccine to provide immunity), therapeutics (i.e., developing drugs to treat and cure the disease), and diagnostics (i.e., developing tests to detect the disease).[2−14] Developing diagnostic tests that can reliably and accurately detect COVID-19 at all stages of infection in a rapid manner is crucial to stopping the spread of the virus and gaining control over the pandemic. There are three main categories for COVID-19 diagnosis, via detection of (1) the nucleic acid genome of the SARS-CoV-2 using qualitative reverse transcriptase polymerase chain reaction (qRT-PCR) and loop-mediated isothermal amplification (LAMP), (2) viral antigens/proteins by the enzyme-linked immunosorbent assay (ELISA) or lateral flow assay (LFA), and (3) antibodies produced by the human immune system.[4,12,14−16] Current Food and Drug Administration (FDA)-approved qRT-PCR, LAMP, ELISA, and ID NOW-COVID-19 (Abbott) diagnostic tests provide false responses at the early stage of infection due to specificity and sensitivity issues. This is partly caused by the low abundance of biomarkers (viral RNA, viral proteins, and antibodies) in the human body.[4,5,7−12,14,17−20] Although RT-PCR is a very accurate diagnostic test, it can take days for the

Received: December 17, 2020
Accepted: June 2, 2021
Published: June 14, 2021

https://doi.org/10.1021/acs.analchem.0c05300
Anal. Chem. 2021, 93, 8754−8763

test results to arrive if sufficient reagents and personnel for testing are not available.[4,5,9,12,14,21] Moreover, there are three major bottlenecks in these existing univariant analytical techniques to precisely and robustly assay COVID-19-associated biomarkers directly in bodily fluids (saliva and blood/plasma/serum) and/or nasal swabs: (1) inability to assay different types of biomolecules in one instrument, for example, the RT-PCR and LAMP techniques are capable of assaying viral nucleic acids but not proteins, whereas (2) ELISA and LFA only detect proteins but not RNAs, and (3) general inadequacy in assay sensitivity/limit of detections to quantify the low abundance of biomarkers while retaining high specificity and accuracy.

To alternate the rate of COVID-19 spread, simultaneous detection of multiple RNA gene sequences, the spike protein of SARS-CoV-2, and plasma antibodies all within one biosensor platform ("multiplex") as well as rapidly processing a large number of patient samples ("high-throughput") all in one instrumental run are crucial. This scheme will have unmatched potential to form precise, early, and rapid diagnostic tests for COVID-19 and quantitate its progression. To the best of our knowledge, such biosensing platforms have not been designed, fabricated, or tested for the SARS-CoV-2 infection. In this context, ultrasensitive detection of COVID-19 biomarkers is very important to differentiate infection before the onset of symptoms between asymptomatic and healthy patients. Early detection itself will clearly reduce spread to the vulnerable elderly. Furthermore, quantitative monitoring of a person's complicated antibody response versus viral load could constitute protocols to reduce the mortality rate through evaluation of potential transmission risk and by providing a measure of disease progression and severity for treatment by clinicians. Deployed on a wide scale in community surveys, it could provide rapid information about immunity and infectious risk in a population and might be particularly useful in places like schools to define the presence of antibodies (suggesting immunity) and infection (suggesting quarantine). Recently, Lechuga and co-workers outlined that nanophotonic biosensors, including those fabricated with plasmonic novel metal nanostructures, have the potential for fast and widespread diagnostic of COVID-19.[4] However, fabrication of a solid-state nanoplasmonic biosensor for highly specific COVID-19 diagnostics has not been reported yet.

In this article, we report a nanoplasmonic-based ultrasensitive and highly specific, label-free screening test for COVID-19 that can detect SARS-CoV-2 RNA genes (4 N genes, the RdRp gene, and the E gene) and spike protein subunits in addition to human antibodies (IgG and IgM) all within one biosensor platform and in a single instrumental run. Therefore, our newly developed nanoplasmonic-based biosensors are capable of detecting all types of COVID-19-related biomarkers.[3−6,14] We utilized the unique localized surface plasmon resonance (LSPR) properties of chemically synthesized gold triangular nanoprisms (Au TNPs) for the construction and spectral response of our biosensors. The nanoplasmonic biosensors are constructed using multiwell plates and cover all three diagnostic testing types (nucleic acid, virus, and antibody) with limits of detection (LODs) for each biomarker as low as 89 aM with excellent specificity. Also, we calculated the dissociation constant (K_D) for different biomolecular interactions using a simple Langmuir equilibrium model or Hill plot equation. In this work, we report the implementation of our detection approach in COVID-19-positive patient plasma sample analysis (n = 80), quantifying both IgG and IgM (serological test) without sample preparation, in a rapid manner (1 h or less). Most importantly, the IgG/IgM levels are highly distinguishable between COVID-19-positive patient plasma samples (n = 80) and healthy individual samples (n = 72) based on robust statistical analyses. Benefiting from the multiplex and high-throughput assay presented herein, we believe that our nanoplasmonic screening test could expedite the detection of COVID-19 at various stages of infection.

EXPERIMENTAL SECTION

Materials. Chloro(triethylphosphine) gold(I) (Et_3PAuCl, 97%) was purchased from Gelest Inc. Poly(methylhydrosiloxane) (PMHS, Mn = 1700−3300), triethylamine (TEA, 98%), 11-mercaptoundecanoic acid (MUDA), 1-nonanethiol (NT), and ACS-grade acetonitrile (CH_3CN, 99.9%) were purchased from Sigma-Aldrich. 3-Mercaptopropyl-trimethoxysilane (MPTMS, 94%) was purchased from Alfa Aesar. Ethanol (200 proof) was purchased from Decon Labs. Thiolated polyethylene glycol (SH-PEG4) was purchased from purePEG. Thiol-modified nucleic acid oligos (-ssDNA-3′-C3-SH) and RNA genes were purchased from Integrated DNA Technologies (IDT). SARS-CoV-2 (COVID-19) spike antibody [CR3022] corresponding to the S1 subunit (sub1) and SARS-CoV/SARS-CoV-2 (COVID-19) spike antibody [1AA9] corresponding to S2 subunit (sub2) were purchased from GeneTex. Human CellExp Coronavirus Spike protein subunit 1 (SARS-CoV-2; sub1) and Human CellExp Coronavirus Spike protein subunit 2 (SARS-CoV-2; sub2) were purchased from Axxora. Anti-SARS-CoV-2 neutralizing antibody, human IgG1 was purchased from Acros Biosystems. Human IgG was purchased from MP Biomedicals, LLC. Goat anti-human IgM was purchased from NOVUS. Human IgM was purchased from Invitrogen. All chemicals were used without further purifications. All COVID-19-related patient samples were collected with Indiana University Institute Review Board approval (IRB Protocol #2004188283). Control plasma samples were collected during the pre-COVID-19 era (2018 or earlier, prior to COVID-19 being present in the USA) by the Indiana University BioBank.

Fabrication of Nanoplasmonic-Based Biosensors for COVID-19. To construct the biosensor, ∼42 nm edge-length Au TNPs were chemically attached onto silanized glass coverslips (see the Supporting Information), followed by performing a tape-cleaning procedure to remove nonprismatic nanostructures. Glass coverslips containing nearly 95 Au TNPs were glued to the bottom of a no-bottom, 96-well plate using a previously published procedure.[22] Briefly, a small amount of glue was applied to the edges of the wells, followed by careful placement of the Au TNP-functionalized coverslip onto the glue area. Gentle pressure was applied to the coverslip for appropriate attachment. The coverslip-attached wells were allowed to dry for at least 1 h at room temperature and then incubated in water for an additional 1 h to confirm that no leakage had occurred. For biosensor construction for SARS-CoV-2 RNA gene detection, each well was incubated in 0.3 mL of a 100:1.0 μM ratio of -ssDNA-3′-C3-SH:PEG4-SH PBS buffer solution overnight, followed by rinsing with a copious amount of phosphate-buffered saline (PBS) buffer to remove loosely bound receptors. For SARS-CoV-2 spike protein subunit detection, each well was incubated in 0.3 mL of ethanolic solution of 100:1.0 (μM) MUDA:NT overnight to

https://doi.org/10.1021/acs.analchem.0c05300
Anal. Chem. 2021, 93, 8754−8763

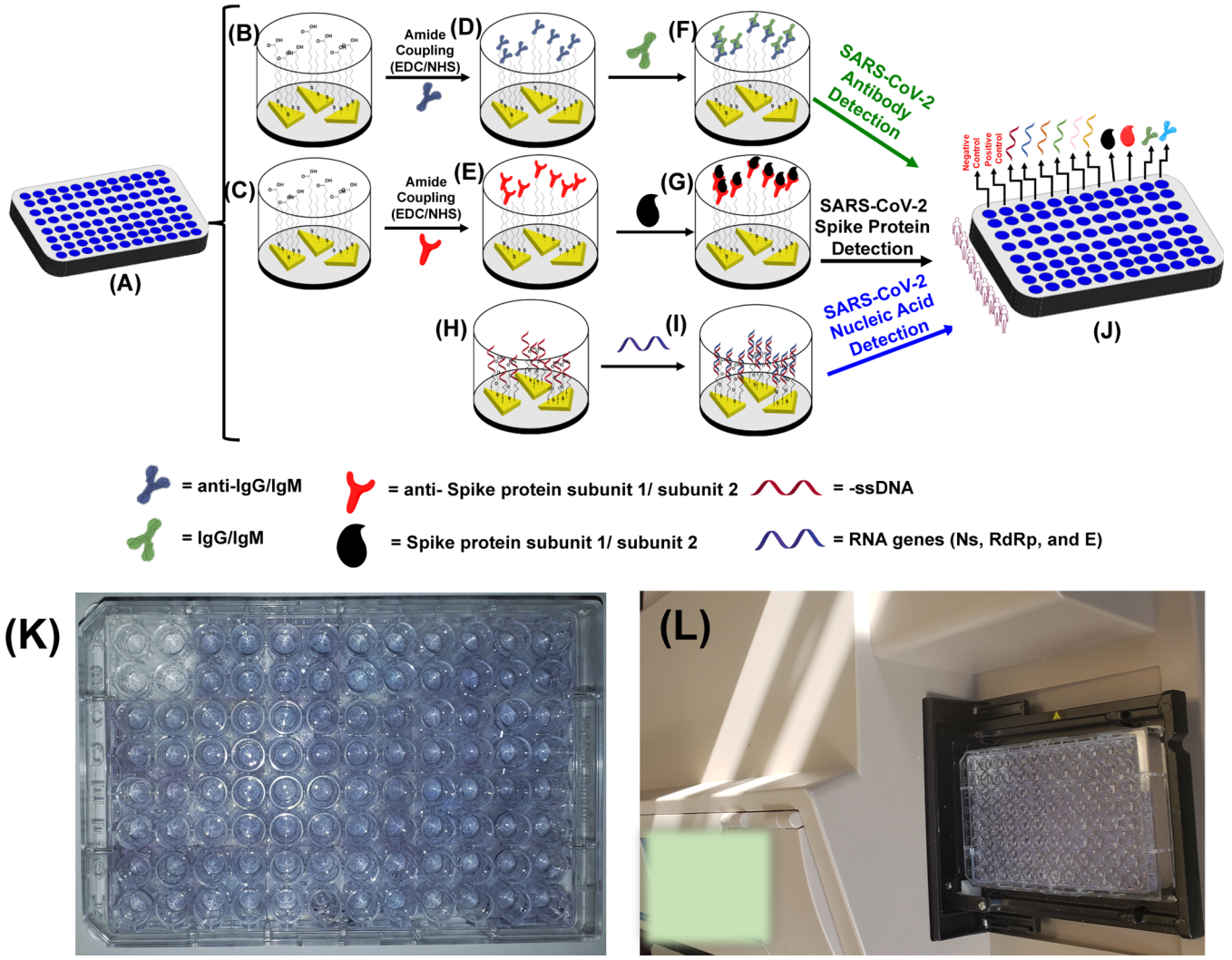

Figure 1. (A–J) Schematic diagram of the fabrication of nanoplasmonic-based, multiplexing COVID-19 diagnostic biosensors. (A) 96-well plate containing glass coverslip-bound Au TNPs. (B,C) Modification of the surface of Au TNPs with MUDA/NT SAMs, followed by amide coupling to attach (D) SARS-CoV-2 anti-IgG/IgM (antigens, anti-IgG/IgM) or (E) anti-spike protein subunit 1 and subunit 2 (antibodies, anti-spike sub 1/sub2) for the detection of (F) IgG/IgM antibody and (G) spike protein subunit 1 and subunit 2, respectively. Au TNPs are functionalized with (H) X-ssDNA-3′-C3-SH and PEG4-SH for (I) RNA gene detection. Therefore, each well represents an individual biosensor in a multiplexed format (J). Picture of a fully fabricated multiplexing and high-throughputs screening test plate (K), which is placed in a plate reader to determine the λ_{LSPR} value (L).

prepare self-assembled monolayers (SAMs). After careful rinsing first with ethanol and then with PBS buffer, each well was incubated in a 0.2 M solution of EDC/NHS in PBS buffer for 2 h and then incubated in a 1.0 μg/mL SARS-CoV-2 (COVID-19) spike antibody (anti-spike subunit1 or subunit2) in PBS buffer overnight. The next day, each well was rinsed with PBS buffer to remove any loosely bound receptors. For IgG and IgM biosensor construction, an identical protocol was followed as described for SARS-CoV-2 spike protein biosensors except that the MUDA/NT SAM-modified TNPs were functionalized with 1.0 μg/mL Anti-SARS-CoV-2 neutralizing antibody IgG1 or IgM (anti-IgG/IgM).

Quantification of Antibody (IgG and IgM) Levels in COVID-19-Positive Patient Plasma. Nanoplasmonic biosensors were incubated in a solution containing 10 μL of COVID-19-positive patient plasma (or normal control, COVID-19-negative patient plasma) diluted with 0.29 mL of PBS buffer for 24 h. Then, the biosensors were thoroughly washed with PBS buffer, and the λ_{LSPR} was recorded for each patient for both IgG and IgM.

RESULTS AND DISCUSSION

Design and Fabrication of the Label-Free COVID-19 Detection Device. Our COVID-19 detection approach utilizes the LSPR response of gold triangular nanoprisms (Au TNPs) that are attached onto glass substrates. Adsorption of analytes onto receptor-functionalized Au TNPs (nanoplasmonic biosensor) results in a local refractive index change that alters their LSPR properties, specifically their λ_{LSPR} position. Our nanoplasmonic biosensors are capable of detecting 3 different types and a total of 10 SARS-CoV-2-related biomarkers in a single instrumental run (Figure 1): (1) four nucleocapsid phosphoprotein genes (N genes-421, 443, 836, and 886) and two structural protein genes (envelope protein-E and RdRP) of SARS-CoV-2; we selected these genes and their nucleic acid segments based on previous literature reports and the Center of Disease Control and Prevention

https://doi.org/10.1021/acs.analchem.0c05300
Anal. Chem. 2021, 93, 8754–8763

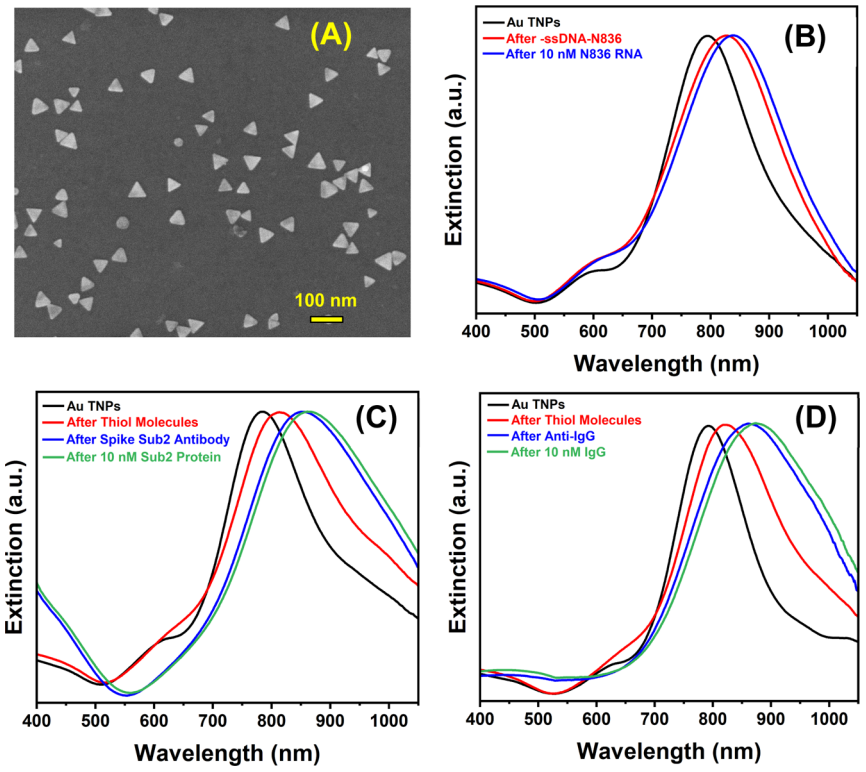

Figure 2. (A) Representative scanning electron microscopy image of ∼42 nm edge length Au TNPs. The scale bar is 100 nm. (B) UV−vis extinction spectra of glass substrate-bound Au TNPs before any surface modification (black curve, 796 nm) and after functionalization with a 100:1 (in μM) ratio of HS-C3-3′-ssDNA-N-836 and HS-PEG4 (red, 831 nm) to prepare biosensors and after incubation of biosensors in 10.0 nM RNA gene N-836 (blue, 843 nm). (C) UV−vis extinction spectra showing change in λ_{LSPR} of Au TNPs before (black, 786 nm) and after functionalization with a 100:1 (in μM) ratio of MUDA/NT SAM (red, 816.9 nm), followed by covalent attachment of anti-spike protein subunit 2 via amide coupling (blue, 855.3 nm), and then incubation of biosensors in 10.0 nM spike sub2 (green, 865.5 nm). (D) UV−vis extinction spectra showing change in λ_{LSPR} of Au TNPs before (black, 786 nm) and after functionalization with a 100:1 (in μM) MUDA/NT SAM (red, 816.9 nm), followed by covalent attachment of anti-IgG (blue, 860.8 nm) via amide coupling, and then incubation of biosensors in a 10.0 nM IgG solution (green, 870.9 nm). All UV−Vis extinction spectra were recorded in PBS buffer (pH = 7.2).

(CDC) guidelines because these genes cover a wide range of the nucleic genomes;[5−7,12−14,23,24] (2) the Spike protein subunits of SARS-CoV-2. These are a set of biomarkers for the detection of the intact virus. Spike proteins are part of the virus' structural surface and are known to bind with the receptor ACE2 in the human body, allowing translocation to the interior of the cells.[3,10,12−16,25] Both subunits 1 and 2 are selected because they cover the majority of the amino acid sequence of the full spike protein (sub1 = 318−510 aa, sub2 = 1029−1192 aa).[14,16,25] (3) Antibodies IgG and IgM are produced due to COVID-19 and can be used in serology tests. Antibodies are excellent biomarkers for determining the level of immune response commonly observed from viral infections, and they serve to neutralize the virus and provide protection to the host from reinfection.[8,9,11,12,21,26−28] Overall, the selected 10 biomarkers for our COVID-19 screening test should cover all stages of the disease development, such as asymptomatic, early infection, overly infected, and post-infection.

The fabrication of our nanoplasmonic test plate for label-free detection of SARS-CoV-2 RNA, spike protein, and human antibodies is described in Figure 1 as follows: chemically synthesized Au TNPs are attached onto MPTMS-functionalized glass substrates, which are glued to the bottom of a no-bottom, 96-well plate (panel A). We adopted two different functionalization approaches to modify the Au TNP surface with specific receptor molecules to detect nucleic acids and proteins. Surface functionalization for protein detection (spike protein subunits and antibodies) was performed by forming a SAM of MUDA and NT (1.0 mM and 10.0 μM concentrations of each solution) (panels B and C), followed by amide coupling with EDC/NHS in the presence of anti-SARS-CoV-2-IgG/IgM (panel D) and spike antibodies (anti-spike) (panel E), which provide IgG/IgM (panel F) and spike protein sub1 and sub 2 (panel G) detection, respectively. Separately, for SARS-CoV-2 viral gene detection, Au TNPs were functionalized with a 100:1 ratio of X-ssDNA-3′-C3-SH and PEG4-SH solution (panel H), which is complementary to a specific target gene sequence (panel I). Overall, the multiwell plate is capable of producing 92 different assemblies with four wells specifically designated for blank references and with each well considered as an individual biosensor (panel J). Therefore, this 96-well system is a multiplex, high-throughput assay. A fully functional multiplexing, high-throughput biosensor is shown in Figure 1K, which is placed in a plate reader to determine the λ_{LSPR} values for each well (Figure 1L). The difference in λ_{LSPR} position before and after the target analyte attachment to the specifically designed biosensors can be utilized to determine the concentration of analytes in COVID-19-positive samples.

We used Au TNPs to fabricate nanoplasmonic biosensors for the COVID-19 diagnostic test due to their extraordinarily high LSPR sensitivity compared to other Au nanostructures such as spherical nanoparticles and nanorods.[29−31] This high LSPR sensitivity arises from large electromagnetic field enhancement at their sharp corners and edges, which causes

https://doi.org/10.1021/acs.analchem.0c05300
Anal. Chem. 2021, 93, 8754−8763

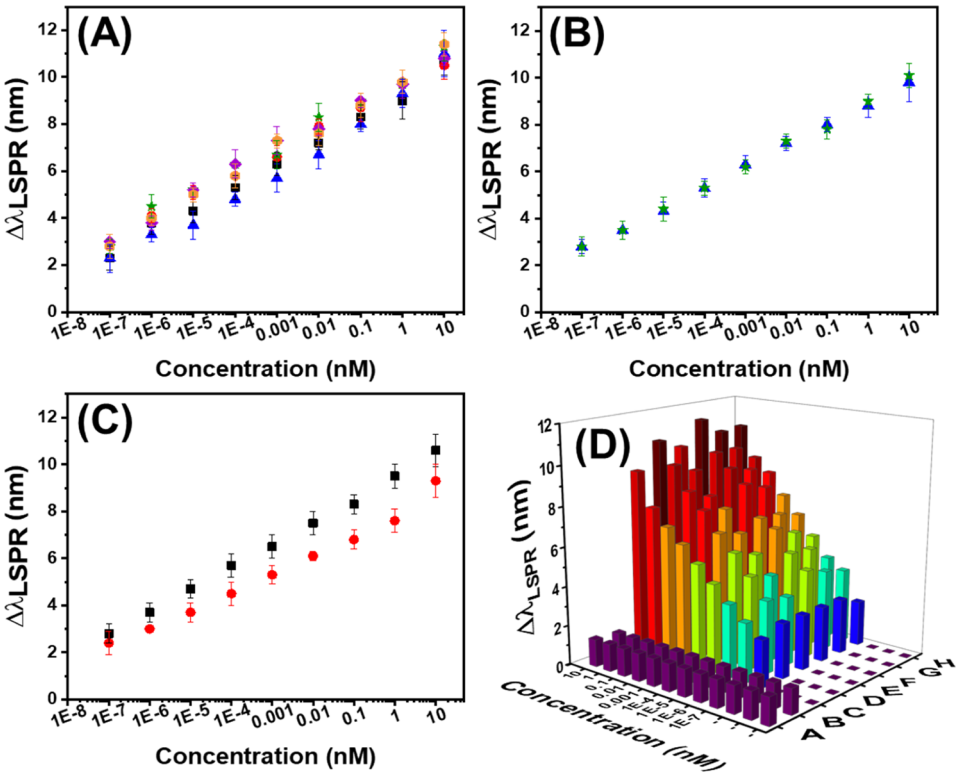

Figure 3. Shift in λ_{LSPR} peak position ($\Delta\lambda_{LSPR}$) of Au TNPs under a nanoplasmonic biosensor construct as a function of different concentrations of the COVID-19 biomarker. The $\Delta\lambda_{LSPR}$ value for (A) six SARS-CoV-2 RNA genes [E gene (black squares), RdRP gene (red circles), N gene-886 (blue triangles), N gene-836 (green stars), N gene-443 (purple diamonds), and N gene-421 (orange hexagons)], (B) spike protein sub1 (blue triangles) and sub2 (green stars), and (C) IgG (black squares) and IgM (red circles) antibodies. Concentrations were plotted in the logarithmic scale to determine nonspecific absorption of endogenous biomolecules from human plasma at a lower concentration range. (D) Three-dimensional representation of average $\Delta\lambda_{LSPR}$ values of COVID-19 biosensors for different concentrations of SARS-CoV-2 viral spike protein, human antibodies, and RNA genes utilizing a 96-well plate in a single instrument run (A = false positive, B = false negative, C= IgM, D = IgG, E = spike sub2, F = N gene-836, G = RdRp gene, and H = E gene). The remaining wells as shown in the last three rows between C and H were unfunctionalized Au TNPs to determine the background of the instrument noise. False negative analysis was conducted by incubating only the SAM-modified Au TNPs (without any receptors) in a 10.0 nM biomarker solution. For the RNA gene and protein detection, Au TNPs were functionalized with PEG4-SH and MUDA/NT SAMs, respectively, for false negative analysis. Purple bars represent $\Delta\lambda_{LSPR}$ values upon incubation of biosensors in human plasma without the biomarker present. These values were used as the blank for LOD calculation. False positive analysis was conducted by incubating the biosensors in a PBS buffer solution without any analytes.

an increase in the polarizability and dipole moment of the electrons, overall providing an increase in the electromagnetic field around the nanoparticle.[32−37] In addition to their unique LSPR properties, Au TNPs possess flat surfaces that allow uniform attachment of receptor molecules via aliphatic chain linkers as a form of SAM that together reduces nonspecific binding of unwanted biomolecules. We previously demonstrated the high sensitivity of Au TNPs for LSPR-based detection of different disease-related microRNAs (pancreatic and bladder cancer)[32,33,38] and protein (cardiac troponinT)[39] using nonmultiplexing assays. Herein, we present the construction of a multiplexing test plate assay that combines both viral RNA and protein and human antibody detection simultaneously. We used ∼42 nm edge length Au TNPs to fabricate the nanoplasmonic biosensors. Figure 2A shows a representative scanning electron microscopy image of Au TNPs attached onto glass substrates. The ∼42 nm edge length TNPs display a λ_{LSPR} at ∼800 nm in acetonitrile (Figure S1).

The silanized glass, coverslip-attached Au TNPs display a λ_{LSPR} at ∼785 nm in PBS buffer (Figure 2B−D black curves). For the SARS-CoV-2 RNA gene detection, the surface of TNPs was modified with an X-ssDNA-3′-C3-S-/PEG4-S- mixture that results in a 32.8 to 35.6 nm red shift of the λ_{LSPR} with X being N-421, -443, -836, -886, E, and RdRp. All nucleic acid gene sequences are provided in the Supporting Information (Table S1). This red shift is due to change in the local dielectric environment of Au TNPs upon attachment of X-ssDNA-3′-C3-S-/PEG4-S-.[40] As shown in Figure 2B, incubation of N836-ssDNA-3′-C3-S-/PEG4-S- modified Au TNPs in a 10.0 nM solution of RNA with an appropriate complementary sequence results in an additional 9.8−11.4 nm red shift of the λ_{LSPR} (Table S2). An example of the LSPR peak shift for SARS-CoV-2 N-836 is shown in Figure 2B. The magnitude of the LSPR shift is in agreement with our previous work on microRNA detection using the same sensing mechanism.[22] This shift is from a combination of change in the local dielectric environment of Au TNPs and delocalization of their excitons within the -ssDNA/RNA duplex.[38] LSPR peak shifts for the other five nucleic acid gene sequences are provided in the Supporting Information (Tables S2 and S4). Detection of spike protein subunits and IgG and IgM of SARS-CoV-2 is shown schematically in Figure 1. The basic nanoplasmonic biosensor construct for detection of these proteins is almost identical except for selecting different receptor molecules for detecting a particular analyte. The presence of MUDA/NT SAMs on Au TNPs produces an

https://doi.org/10.1021/acs.analchem.0c05300
Anal. Chem. 2021, 93, 8754−8763

~λ_{LSPR} red shift of 30.7 ± 3.1 nm due to change in the local dielectric environment.[41] Covalent attachment of anti-spike protein sub1 and sub2 via amide coupling results in additional 37.9 ± 1.6 and 38.3 ± 0.4 nm λ_{LSPR} red shifts, respectively. This step completes the assembly of nanoplasmonic biosensors for SARS-CoV-2 spike protein detection. Incubation of this biosensor in 10.0 nM spike protein sub1 and sub2 provides average λ_{LSPR} red shifts of 9.8 and 10.1 nm, respectively (Figures 2C and S2). To detect human antibodies, anti-IgG and IgM were covalently attached to MUDA/NT SAM-modified TNPs via amide coupling that results in λ_{LSPR} red shifts of 39.7 and 39.3 nm, respectively. This step produces biosensors for IgG and IgM detection. When nanoplasmonic biosensors were incubated in 10.0 nM IgG and IgM solutions, they produce average λ_{LSPR} red shifts of 10.6 and 9.3 nm, respectively (Figures 2D and S3).

COVID-19 Biomarker Assays. We developed calibration curves for all biomarkers in human plasma by incubating biosensors in an individual well with varying concentrations of the biomolecules. The multiplexing capability of our COVID-19 nanoplasmonic screening test allows the development of multiple calibration curves in a single 96-well format where each well in a column is designated for a different concentration of the same biomarker. The calibration curves resulted in a linear range of 10 nM to 100 aM for each biomarker with $R^2 > 0.985$ (Figure 3A–C, Tables S3 and S4). For SARS-CoV-2 RNA gene sequence detection, calculated LODs range between 90 and 980 aM (Table S3). Our LODs for SARS-CoV-2 RNA detection are 10^2 to 10^6 times better than those reported in the literature for the laboratory-based technique (220 fM and 29.2 nM).[5,6,23] Although Tian et al. reported an LOD of 400 aM for only RdRp via an optomagnetic-based approach, the method requires RNA amplification to achieve this LOD value.[23] In contrast, our LSPR-based detection of RNA does not require any pre-amplification protocols. Our LODs of SARS-CoV-2 sub1 and sub2 detection are 211 and 246 aM, respectively (Table S3). These LODs are comparable to those reported in the literature of 13.1 aM for sub1 using electrochemical approaches.[10,16] Electrochemical-based biosensors are notorious for providing false responses in real biological matrixes. Finally, we determined LODs of 170 aM and 1.0 fM for IgG and IgM, respectively (Table S3). We believe that this relatively high LOD for IgM could be from their extremely large size (molecular weight ~950 kDa) that restricts attachment of many IgM molecules onto the biosensor surface from the steric repulsion. Many absorbance- and fluorescence-based techniques have recently been developed for specific SARS-CoV-2 antibody assays, and these techniques can only detect IgG and/or IgM and are not capable of quantifying these biomarkers.[8,9,11,12,21,26] Funari et al. reported an LOD of 0.5 pM for IgG,[27] and Ma and co-workers determined LODs of 33.3 and 20.6 fM for IgG and IgM detection, respectively;[28] however, our LSPR-based detection provides an LOD at least 20 times better than these reports. We also tested false positive and false negative responses (see the Experimental Section for details) in the multiplexed setup (Figure 3D). We observe a maximum $\Delta\lambda_{LSPR}$ of 1.6 nm, which is at least 1.0 nm lower than the lowest biomarker concentration (100 aM) (Table S4). These false positive and false negative results indicate that our multiplexed COVID-19 screening test should be highly specific and sensitive at detecting SARS-CoV-2, respectively. Together, the LOD values in the fM and aM ranges for nucleic acid RNA detection, viral protein detection, and antibody detection using our nanoplasmonic biosensors suggest that our diagnostic test can be used for early detection as well as for other stages of infection with high selectivity. Further specificity tests are described below.

The results provided above suggest that the interaction between the receptor and analyte molecules is highly specific. Most importantly, the calibration curves show at least 8 order of magnitude linearity. Therefore, one must consider that these are strong receptor–analyte interactions and utilizing such interactions is crucial for developing highly effective and selective biosensors. To further characterize this interaction, we determined the dissociation constant (K_D) for each biomarker in our biosensor utilizing a Langmuir equilibrium model for RNA gene sequences and Hill plots for proteins (spike protein subunits and antibodies). Additional information for the determination of K_D is provided in the Supporting Information, Figures S4 and S5 and Table S5. The K_D value ranges between 1.27 and 1.47 × 10^{-10} M for SARS-CoV-2 genes. Our LSPR-based determination of K_D values is in good agreement with literature reports on DNA/RNA interactions.[5,42] The K_D value in the 10^{-10} M range suggests that there is a strong affinity for selected SARS-CoV-2 RNA gene sequences toward our designed receptor molecules. As illustrated in Figure S5A,B, K_D values of 1.42 × 10^{-12} and 1.51 × 10^{-11} M are determined for SARS-CoV-2 spike protein sub1 and sub2, respectively. Both spike protein subunits show strong interactions; however, the smaller K_D value for sub1 indicates that it may be a better biomarker for SARS-CoV-2 spike protein detection than sub2 utilizing our nanoplasmonic biosensor construct. Although a K_D value of 9.55 × 10^{-12} M for IgG is determined under our experimental conditions, IgM produces relatively weaker binding (a K_D value of 3.33 × 10^{-7} M) (Figure S5C,D). We believe this larger K_D for IgM is due to the hindered interaction between surface-bound receptors (anti-IgM) and IgM. A plausible reason for such inadequacy is the steric repulsion from the bulky IgM protein. Nevertheless, our calculated K_D value for IgG is in good agreement with a recent report of 8.0 × 10^{-12} M, which also utilized an LSPR-based method.[27] It is important to mention that both the Langmuir equilibrium and Hill plot models take into consideration that the interaction between large biomolecules such as two proteins is homogeneous such that one surface site of the biomolecule of interest (e.g., antigen) binds to one antibody site. Although such an assumption should be true for our anti-IgG/IgG interaction, it may not be fully accurate for the SARS-CoV-2 spike glycoprotein. Recently, Fornstedt and co-workers showed that a thorough quantitative model is required to determine the K_D values for the SARS-CoV-2 receptor binding domain (RBD) interaction with angiotensin-converting enzyme 2 (ACE2).[43] It is important to mention that the K_D values we determined for sub1 and sub2 are based on using a fully complimentary receptor, whereas the interaction between SARS-CoV-2 RBD and ACE2 is part of two different biological compartments, and their interaction can be varied depending on the actual structure of SARS-CoV-2 S glycoprotein. Nevertheless, our reported K_D values for different biomolecular interactions are based on simple binding models, and perhaps, further analysis could be done by scientists who are working on the development of rigorous interaction models.[44] Taken together, the smaller K_D values explicitly suggest that the interaction between the biomarkers and receptors is strong, and thus, our chosen multiple

https://doi.org/10.1021/acs.analchem.0c05300
Anal. Chem. 2021, 93, 8754–8763

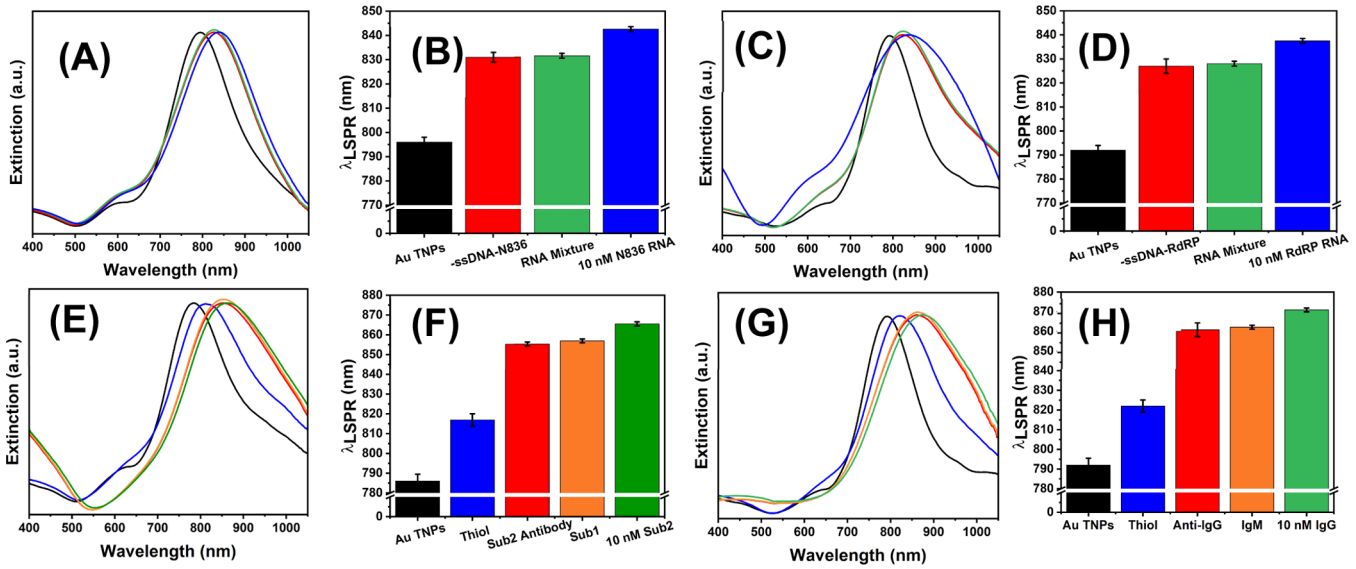

Figure 4. Specificity test of nanoplasmonic biosensors for different SARS-CoV-2 biomarkers. UV−vis extinction spectra (A) and bar graph (B) of Au TNPs before (black curve/black bar, λ_{LSPR} = 796.0 nm) and after functionalization with HS-C3-3′-ssDNA-N-836 and HS-PEG4 (red curve/red bar, λ_{LSPR} = 831.1 nm) and after incubation in a mixed solution of a 10.0 nM concentration of N-886, N-421, N-443, RdRP, E, and CDC recommended probe genes (green curve/green bar, λ_{LSPR} = 831.6 nm). The biosensors were properly washed with PBS buffer before incubation in a 10.0 nM N-836 gene solution (blue curve/blue bar, λ_{LSPR} = 842.6 nm). UV−vis extinction spectra (C) and bar graph (D) of λ_{LSPR} Au TNPs before (black curve/bar, λ_{LSPR} = 792.0 nm) and after functionalization with HS-C3-3′-ssDNA-RdRp and HS-PEG4 (red curve/bar, λ_{LSPR} = 827.0 nm) and then incubation in a mixed solution of a 10.0 nM concentration of N-836, N-886, N-421, N-443, E, and CDC recommended SARS-CoV-specific genes (green curve/bar, λ_{LSPR} = 828.0 nm) and finally after incubation in 10.0 nM RdRP gene solution (blue curve/bar, λ_{LSPR} = 837.5 nm). UV−vis extinction spectra (E) and bar graph (F) of Au TNPs before (black curve/bar, λ_{LSPR} = 786.0 nm) and after mixed MUDA/NT SAM (blue curve/bar, λ_{LSPR} = 816.9 nm) functionalization after covalent attachment of anti-spike subunit 2 (red curve/bar, λ_{LSPR} = 855.3 nm) and then incubation in a 10.0 nM spike sub1 solution (orange curve/bar, λ_{LSPR} = 856.9 nm) and finally after incubation in a 10.0 nM spike sub2 solution (green curve/bar, λ_{LSPR} = 865.5 nm). UV−vis extinction spectra (G) and bar graph (H) of Au TNPs before (black curve/bar, λ_{LSPR} = 792.0 nm) and after mixed MUDA/NT SAM (blue curve/bar, λ_{LSPR} = 822.0 nm) functionalization and after covalent attachment of an anti-IgG via EDC/NHS coupling (red curve/bar, λ_{LSPR} = 860.8 nm). The biosensors then incubated in a 10.0 nM IgM solution (orange curve/bar, λ_{LSPR} = 862.1 nm). The biosensors then incubated in a 10.0 nM IgG solution (green curve/bar, λ_{LSPR} = 870.9 nm). All extinction spectra were recorded in PBS buffer (pH 7.2). Curve fitting through Origin software was applied to determine the exact λ_{LSPR} value. Error bars represent the value measured from three different wells of the same biosensor construct.

biomarkers can be utilized for highly specific and sensitive detection of the SARS-CoV-2 and relevant antibodies for COVID-19 and for diagnostic and prognosis purposes.

Specificity Tests of Nanoplasmonic Biosensors for COVID-19 Diagnostics. Unprecedentedly high specificity of any newly developed diagnostic device is the key to mitigate false positive results. This is true for COVID-19 diagnostic tests; however, many existing assays produce false responses at the disease onset due to lack of specificity. The high sensitivity of our nanoplasmonic-based COVID-19 screening test has caused us to further examine the specificity of our multiplexed assay. We performed specificity tests for all 10 biomarkers, as shown in Figures 4 and S6−S8. As described above, each well (biosensor) is carefully designed to detect a very specific biomarker. In the specificity test, a single biosensor was incubated in a mixture of similar types of biomolecules excluding the one that is fully complimentary to the receptor of the sensor. Figure 4A,B shows an example of the result for the SARS-CoV-2 N-836 sequence. Functionalization of Au TNPs with N836-ssDNA-3′-C3-S-/PEG4-S- produces a λ_{LSPR} value of 831.1 nm (Figure 4A, red curve). This biosensor should be very specific to the detection of the SARS-CoV-2 N-836 gene because all other genes are noncomplementary and thus should not bind to the biosensor. The biosensor was then incubated in a 10.0 nM mixture of N-886, -421, -443, RdRP, and E genes that results in a λ_{LSPR} of 833.0 nm (Figure 4A, green curve). Thus, a negligible change in the $\Delta\lambda_{LSPR}$ value of ∼2.0 nm indicates no N-gene hybridization to the -ssDNA-N-836 or likely due to transient base−pair interactions. The minimal observed shift could be due to instrumental noise. Next, an identical biosensor was incubated in a 10.0 nM solution of N-836, and a λ_{LSPR} value of 842.6 nm ($\Delta\lambda_{LSPR}$ = 11.5 nm, Figure 4B) is observed (Figure 4A, blue curve). The LSPR data suggest successful interactions between the Au TNP bound -ssDNA-N-836 and N-836 gene sequences of SARS-CoV-2. The nucleocapsid phosphoprotein gene (N-gene) and RdRp gene nucleic acid genomes are very large; therefore, we performed additional specificity tests with different nucleic acid sequences within each gene (Table S1). We selected the N-gene specificity RNA sequence because it is fully complimentary to a qRT-PCR -ssDNA probe used for detecting COVID-19 based on the Centers for Disease Control and Prevention (CDC) recommendation.[45] Additionally, the RdRp-specific RNA sequence was selected because this particular RNA sequence is found in the SARS-CoV virus but not in SARS-CoV-2.[6] Since the two viruses have similar nucleic acid genomes, choosing a sequence in the SARS-CoV virus that is not found in SARS-CoV-2 will fully demonstrate the specificity of our nanoplasmonic biosensors for detecting COVID-19. As illustrated in Figure 4C,D, our biosensors display high specificity toward the RdRp gene. The additional specificity that results for other N (N-886, N-421, and N-443)

https://doi.org/10.1021/acs.analchem.0c05300
Anal. Chem. 2021, 93, 8754−8763

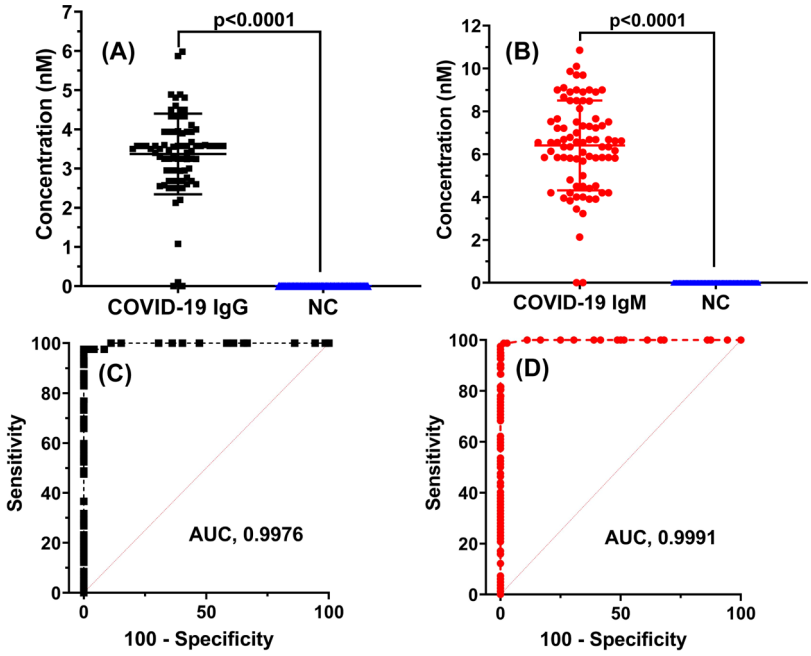

Figure 5. SARS-CoV-2 antibody quantification in 80 COVID-19-positive patient plasma samples. The Mann−Whitney nonparametric test results of normal control (NC = 72) versus COVID-19-positive patient samples (N = 80) for (A) IgG and (B) IgM antibodies. (Black squares = IgG, red circles = IgM). p (ns) = 0.1234, *P < 0.0332,**P < 0.0021, ***P < 0.0002, ****P < 0.0001. ROC curve of normal control versus COVID-19-positive patient samples of IgG (C) and IgM (D).

and E genes is provided in Figure S6. We also performed specificity tests for spike protein sub2 (Figure 4E,F) and IgG (Figure 4G,H). Additional results relevant to sub1 and IgM are provided in the Supporting Information (Figure S8). Taken together, our newly developed nanoplasmonic biosensors for the detection of COVID-19 show extraordinary specificity. Moreover, if one could implement all 10 biomarkers for a single patient, it is can be said with confidence that we can avoid false responses and identify individuals who are asymptomatic with COVID-19. We should also be able to monitor staging of physiological response to optimize patient care.

COVID-19 Patient Plasma Assay for IgG and IgM Detection and Quantification. Serological tests for detection of SARS-CoV-2-specific antibodies (e.g., IgG and IgM) in patient biofluids such as plasma, serum, or whole blood are crucial to determine active and post infection and contact tracing. It is reported that after a week of active infection, both IgG and IgM can be detected. Importantly, IgM levels go down post infection, while IgG levels remain the same even after 5 weeks of initial infection.[46] In addition, quantifying the concentration of IgG and IgM to determine the antibody level in patients would provide insight into the human immune response when overcoming COVID-19 infection and will be critical to epidemiology when mass vaccination occurs. As a proof of concept, we performed serological tests to quantify IgG and IgM levels in COVID-19 patient samples utilizing our biosensors. We obtained 80 COVID-19-positive patient plasma samples from an ongoing study of antibody responses to SARS-CoV-2. All samples were positive by the commercial Abbott Architect test, which measures IgG to the SARS-CoV-2 nucleocapsid antigen. An additional 72 plasma samples (healthy individuals, COVID-19-negative from 2018 or earlier, prior to COVID-19 being present in USA) were also analyzed as normal controls. Due to the unique high-throughput and multiplexing capabilities of our diagnostic test, we are able to quantify both IgG and IgM for 15 COVID-19-positive patient samples in triplicate in a single instrumentation run. Importantly, for each well, only 10 μL of the patient's plasma was used for the antibody detection. As shown in Figure 5, our diagnostic test is capable of quantifying IgG and IgM in COVID-19-positive patients and healthy individuals with the ROC-AUC equal to 0.997 for IgG and 0.999 for IgM at 95% confidence interval. Additionally, the Mann−Whitney nonparametric test provides p < 0.0001 for both IgG and IgM when comparing COVID-19-positive patients (n = 80) with healthy individuals (n = 72). The screening test also provides a calculated sensitivity of 100% (80/80), indicating the ability of the test to identify individuals that have SARS-CoV-2 antibodies (true positive rate). The calculated specificities of 97.3 (78/80) and 96% (77/80) for IgM and IgG, respectively, determined from our test suggest the unique ability of our diagnostic assay to identify individuals without SARS-CoV-2 antibodies (true negative rate). As illustrated in Table S6, these statistical analyses of our nanoplasmonic biosensor-based detection are comparable to those reported in the literature. Most importantly, to the best of our knowledge, this is the first label-free technique to determine both IgG and IgM concentration levels in COVID-19-positive patients. We also performed additional statistical analysis on our diagnostic test to calculate positive and negative predictive values, commonly found in FDA emergency-authorized diagnostic tests for COVID-19. Positive and negative predictive values are calculated using the test's sensitivity and specificity and a "prevalence" which is an assumption about the percentage of individuals in the population who have antibodies to SARS-CoV-2. The calculated positive predictive value (PPV) and negative predictive value (NPV) of our diagnostic test were 98 and 100%, respectively, at the FDA-assumed 5% prevalence. To our knowledge, there is no literature report available

https://doi.org/10.1021/acs.analchem.0c05300
Anal. Chem. 2021, 93, 8754−8763

presenting PPV and NPV of IgG and IgM individually at 5% prevalence. Because of our laboratory safety rating, we are only able to test antibodies from COVID-19 patient samples but no viral RNA and spike protein detection; however, we are confident that our multiplexing diagnostic test will allow quantitative determination of SARS-CoV-2 genes and spike protein from patients with active infection. Although we have demonstrated the serological tests for COVID-19 patient plasma samples, our nanoplasmonic biosensors are also expected to perform antibody detection in positive COVID-19 patient saliva specimens with high efficiency. This is important because saliva testing is noninvasive and thus the entire assay can be conducted quickly. We will report these results separately utilizing a large sample cohort. In addition, we should mention that a limitation to this study includes a relatively small cohort of COVID-19-positive (n = 80) and COVID-19-negative (n = 72) patient samples, which does not allow us to develop a more quantitative model for antibody levels at different stages of infection (early vs post infection). As mentioned above, we aim to expand our research, specifically in serology testing with a larger cohort in a wide spectrum of stages of infection to address the following questions: (1) How long IgG and IgM remain in the bloodstream? (2) Which antibody plays the most crucial role to build long-term immunity? (3) What are the levels of these antibodies in reinfected patients?

CONCLUSIONS

In summary, we have developed the first multiplexed and high-throughput COVID-19 screening test platform by fabricating selective label-free nanoplasmonic biosensors. Our nanoplasmonic biosensors are capable of quantitatively detecting 10 different COVID-19 biomarkers including 6 gene sequences, 2 spike protein subunits, and 2 antibodies of SARS-CoV-2 with aM limit of detections, all within one multiwell plate format and in a single instrumentation run. Additionally, the screening test shows high specificity, which is the key to avoiding false positive responses. Just as importantly, the test showed the potential to quantify both IgG and IgM antibodies directly from plasma of COVID-19-positive patients without requiring sample preparation and from as little as 10 μL of plasma, with an ROC-AUC of >0.990 for both antibodies. The Mann−Whitney nonparametric test provides p-values of <0.0001 for both IgG and IgM for a cohort of 80 COVID-19-positive patients. Additionally, our test also provides unprecedentedly high sensitivity and specificity as well as PPV and NPV >98% at the FDA-approved 5% prevalence.

Despite the limitation of not demonstrating viral RNA and spike protein detection in actual COVID-19 patients' samples and a small cohort size for the antibody assay, we believe that our simple but highly sensitive and specific detection approach should be more effective in identifying active infection by quantifying SARS-CoV-2 gene sequences and spike protein subunits at a very early stage, providing some relief to the burden currently caused from PCR-based testing that is complicated and takes few days to obtain the results. Furthermore, detection of viral-induced antibodies provides a measure of the patient's physiological response to infection and may help in individual treatment of patients. In addition to its current applicability to diagnose new cases of SARS-CoV-2 infection, we also believe that the development of this highly sensitive and specific COVID-19 detection approach, specifically the nanoplasmonic-based serological assay, will be of the upmost importance by analyzing the antibody response throughout the course of infection and when mass vaccine will take place because monitoring the human immune response toward vaccines through quantification of antibodies will be critical to epidemiology.

ASSOCIATED CONTENT

Supporting Information

The Supporting Information is available free of charge at https://pubs.acs.org/doi/10.1021/acs.analchem.0c05300.

Additional experimental details, nucleic acid gene sequences, data processing and statistical analysis, binding constant determination, UV−vis absorption spectra, adsorption isotherms, extinction spectra and bar graphs for specificity tests, raw LSPR peak shift values, LOD values, binding constants, and comparison of different assays for the detection of COVID-19 antibodies (PDF)

AUTHOR INFORMATION

Corresponding Author

Rajesh Sardar − *Department of Chemistry and Chemical Biology, Indiana University-Purdue University Indianapolis, Indianapolis, Indiana 46202, United States; Integrated Nanosystems Development Institute, Indiana University-Purdue University Indianapolis, Indianapolis, Indiana 46202, United States;* orcid.org/0000-0001-9680-1301; Email: rsardar@iupui.edu

Authors

Adrianna N. Masterson − *Department of Chemistry and Chemical Biology, Indiana University-Purdue University Indianapolis, Indianapolis, Indiana 46202, United States*

Barry B. Muhoberac − *Department of Chemistry and Chemical Biology, Indiana University-Purdue University Indianapolis, Indianapolis, Indiana 46202, United States*

Adnan Gopinadhan − *Ryan White Center for Pediatric Infectious Diseases and Global Health, Indiana University School of Medicine, Indianapolis, Indiana 46205, United States*

David J. Wilde − *Department of Chemistry and Chemical Biology, Indiana University-Purdue University Indianapolis, Indianapolis, Indiana 46202, United States*

Frédérique T. Deiss − *Department of Chemistry and Chemical Biology, Indiana University-Purdue University Indianapolis, Indianapolis, Indiana 46202, United States;* orcid.org/0000-0002-8626-5370

Chandy C. John − *Ryan White Center for Pediatric Infectious Diseases and Global Health, Indiana University School of Medicine, Indianapolis, Indiana 46205, United States*

Complete contact information is available at: https://pubs.acs.org/10.1021/acs.analchem.0c05300

Notes

The authors declare no competing financial interest.

ACKNOWLEDGMENTS

We gratefully acknowledge the National Science foundation for financial support of the experimental part of the research through grant CBET-1604617 and IUPUI-OVCR Bridge funding. This work was supported in part by the Indiana

Biobank and the Indiana Clinical and Translational Sciences Institute and funded in part by award no UL1TR002529 from the National Institutes of Health, the National Center for Advancing Translational Sciences, and the Clinical and Translational Sciences Award. The content is solely the responsibility of the authors and does not necessarily represent the official views of the National Institutes of Health.

REFERENCES

(1) Coronavirus Resource Center. https://coronavirus.jhu.edu/map.html (accessed 11 Nov 2020).web
(2) Lin, Q.; Wen, D.; Wu, J.; Liu, L.; Wu, W.; Fang, X.; Kong, J. *Anal. Chem.* **2020**, *92*, 9454−9458.
(3) Ventura, B. D.; Cennamo, M.; Minopoli, A.; Campanile, R.; Censi, S. B.; Terracciano, D.; Portella, G.; Velotta, R. *ACS Sens.* **2020**, *5*, 3043−3048.
(4) Soler, M.; Estevez, M. C.; Cardenosa-Rubio, M.; Astua, A.; Lechuga, L. M. *ACS Sens.* **2020**, *5*, 2663−2678.
(5) Moitra, P.; Alafeef, M.; Dighe, K.; Frieman, M. B.; Pan, D. *ACS Nano* **2020**, *14*, 7617−7627.
(6) Qiu, G.; Gai, Z.; Tao, Y.; Schmitt, J.; Kullak-Ublick, G. A.; Wang, J. *ACS Nano* **2020**, *14*, 5268−5277.
(7) Wang, J.; Cai, K.; Zhang, R.; He, X.; Shen, X.; Liu, J.; Xu, J.; Qiu, F.; Lei, W.; Wang, J.; Li, X.; Gao, Y.; Jiang, Y.; Xu, W.; Ma, X. *Anal. Chem.* **2020**, *92*, 9399−9404.
(8) Chen, Z.; Zhang, Z.; Zhai, X.; Li, Y.; Lin, L.; Zhao, H.; Bian, L.; Li, P.; Yu, L.; Wu, Y.; Lin, G. *Anal. Chem.* **2020**, *92*, 7226−7231.
(9) Feng, M.; Chen, J.; Xun, J.; Dai, R.; Zhao, W.; Lu, H.; Xu, J.; Chen, L.; Sui, G.; Cheng, X. *ACS Sens.* **2020**, *5*, 2331−2337.
(10) Seo, G.; Lee, G.; Kim, M. J.; Baek, S.-H.; Choi, M.; Ku, K. B.; Lee, C.-S.; Jun, S.; Park, D.; Kim, H. G.; Kim, S.-J.; Lee, J.-O.; Kim, B. T.; Park, E. C.; Kim, S. I. *ACS Nano* **2020**, *14*, 12257−12258.
(11) Alves, D.; Curvello, R.; Henderson, E.; Kesarwani, V.; Walker, J. A.; Leguizamon, S. C.; McLiesh, H.; Raghuwanshi, V. S.; Samadian, H.; Wood, E. M.; McQuilten, Z. K.; Graham, M.; Wieringa, M.; Korman, T. M.; Scott, T. F.; Banaszak Holl, M. M.; Garnier, G.; Corrie, S. R. *ACS Sens.* **2020**, *5*, 2596−2603.
(12) Udugama, B.; Kadhiresan, P.; Kozlowski, H. N.; Malekjahani, A.; Osborne, M.; Li, V. Y. C.; Chen, H.; Mubareka, S.; Gubbay, J. B.; Chan, W. C. W. *ACS Nano* **2020**, *14*, 3822−3835.
(13) Liu, C.; Zhou, Q.; Li, Y.; Garner, L. V.; Watkins, S. P.; Carter, L. J.; Smoot, J.; Gregg, A. C.; Daniels, A. D.; Jervey, S.; Albaiu, D. *ACS Cent. Sci.* **2020**, *6*, 315−331.
(14) Iravani, S. *Mater. Adv.* **2020**, *1*, 3092.
(15) Huang, L.; Ding, L.; Zhou, J.; Chen, S.; Chen, F.; Zhao, C.; Xu, J.; Hu, W.; Ji, J.; Xu, H.; Liu, G. L. *Biosens. Bioelectron.* **2021**, *171*, 112685.
(16) Mavrikou, S.; Moschopoulou, G.; Tsekouras, V.; Kintzios, S. *Sensors* **2020**, *20*, 3121.
(17) Coronavirus Disease 2019 Testing Basics. https://www.fda.gov/consumers/consumer-updates/coronavirus-disease-2019-testing-basics (accessed 11 Nov 2020).web
(18) Basu, A.; Zinger, T.; Inglima, K.; Woo, K.-m.; Atie, O.; Yurasits, L.; See, B.; Aguero-Rosenfeld, M. E. *J. Clin. Microbiol.* **2020**, *58*, No. e01136.
(19) Smithgall, M. C.; Scherberkova, I.; Whittier, S.; Green, D. A. *J. Clin. Virol.* **2020**, *128*, 104428.
(20) Pokhrel, P.; Hu, C.; Mao, H. *ACS Sens.* **2020**, *5*, 2283−2296.
(21) Zeng, L.; Li, Y.; Liu, J.; Guo, L.; Wang, Z.; Xu, X.; Song, S.; Hao, C.; Liu, L.; Xin, M.; Xu, C. *Mater. Chem. Front.* **2020**, *4*, 2000−2005.
(22) Masterson, A. N.; Liyanage, T.; Kaimakliotis, H.; Gholami Derami, H.; Deiss, F.; Sardar, R. *Anal. Chem.* **2020**, *92*, 9295−9304.
(23) Tian, B.; Gao, F.; Fock, J.; Dufva, M.; Hansen, M. F. *Biosens. Bioelectron.* **2020**, *165*, 112356.
(24) Zhu, X.; Wang, X.; Han, L.; Chen, T.; Wang, L.; Li, H.; Li, S.; He, L.; Fu, X.; Chen, S.; Xing, M.; Chen, H.; Wang, Y. *Biosens. Bioelectron.* **2020**, *166*, 112437.
(25) Cai, Y.; Zhang, J.; Xiao, T.; Peng, H.; Sterling, S. M.; Walsh, R. M., Jr.; Rawson, S.; Rits-Volloch, S.; Chen, B. *Science* **2020**, *369*, 1586−1592.
(26) Cady, N. C.; Tokranova, N.; Minor, A.; Nikvand, N.; Strle, K.; Lee, W. T.; Page, W.; Guignon, E.; Pilar, A.; Gibson, G. N. *Biosens. Bioelectron.* **2021**, *171*, 112679.
(27) Funari, R.; Chu, K.-Y.; Shen, A. Q. *Biosens. Bioelectron.* **2020**, *169*, 112578.
(28) Wang, Z.; Zheng, Z.; Hu, H.; Zhou, Q.; Liu, W.; Li, X.; Liu, Z.; Wang, Y.; Ma, Y. *Lab Chip* **2020**, *20*, 4255−4261.
(29) Joshi, G. K.; McClory, P. J.; Muhoberac, B. B.; Kumbhar, A.; Smith, K. A.; Sardar, R. *J. Phys. Chem. C* **2012**, *116*, 20990−21000.
(30) Joshi, G. K.; McClory, P. J.; Dolai, S.; Sardar, R. *J. Mater. Chem.* **2012**, *22*, 923−931.
(31) Mayer, K. M.; Hafner, J. H. *Chem. Rev.* **2011**, *111*, 3828−3857.
(32) Joshi, G. K.; Deitz-McElyea, S.; Liyanage, T.; Lawrence, K.; Mali, S.; Sardar, R.; Korc, M. *ACS Nano* **2015**, *9*, 11075−11089.
(33) Joshi, G. K.; Deitz-McElyea, S.; Johnson, M.; Mali, S.; Korc, M.; Sardar, R. *Nano Lett.* **2014**, *14*, 6955−6963.
(34) Hao, E.; Schatz, G. C. *J. Chem. Phys.* **2004**, *120*, 357−366.
(35) Jain, P. K.; El-Sayed, M. A. *J. Phys. Chem. C* **2007**, *111*, 17451−17454.
(36) Nusz, G. J.; Curry, A. C.; Marinakos, S. M.; Wax, A.; Chilkoti, A. *ACS Nano* **2009**, *3*, 795−806.
(37) Zhao, J.; Pinchuk, A. O.; McMahon, J. M.; Li, S.; Ausman, L. K.; Atkinson, A. L.; Schatz, G. C. *Acc. Chem. Res.* **2008**, *41*, 1710−1720.
(38) Liyanage, T.; Masterson, A. N.; Oyem, H. H.; Kaimakliotis, H.; Nguyen, H.; Sardar, R. *Anal. Chem.* **2019**, *91*, 1894−1903.
(39) Liyanage, T.; Sangha, A.; Sardar, R. *Analyst* **2017**, *142*, 2442−2450.
(40) Anker, J. N.; Hall, W. P.; Lyandres, O.; Shah, N. C.; Zhao, J.; Van Duyne, R. P. *Nat. Mater.* **2008**, *7*, 442−453.
(41) Joshi, G. K.; Smith, K. A.; Johnson, M. A.; Sardar, R. *J. Phys. Chem. C* **2013**, *117*, 26228−26237.
(42) Su, Q.; Vogt, S.; Nöll, G. *Langmuir* **2018**, *34*, 14738−14748.
(43) Forssén, P.; Samuelsson, J.; Lacki, K.; Fornstedt, T. *Anal. Chem.* **2020**, *92*, 11520−11524.
(44) Forssén, P.; Multia, E.; Samuelsson, J.; Andersson, M.; Aastrup, T.; Altun, S.; Wallinder, D.; Wallbing, L.; Liangsupree, T.; Riekkola, M.-L.; Fornstedt, T. *Anal. Chem.* **2018**, *90*, 5366−5374.
(45) CDC. *2019 Novel Coronavirus (2019-nCoV) Real-Time rRT-PCR Panel Primers and Probes*; U.S. Department of Health and Human Services, 2020; pp 1−2. Online.
(46) Mattioli, I. A.; Hassan, A.; Oliveira, O. N., Jr.; Crespilho, F. N. *ACS Sens.* **2020**, *5*, 3655−3677.

https://doi.org/10.1021/acs.analchem.0c05300
Anal. Chem. 2021, 93, 8754−8763